



HAL
open science

Modeling of turbulent fluid flow over a rough wall with or with outsuction

G. Grégoire, Michel Favre-Marinet, François Julien Saint Amand

► **To cite this version:**

G. Grégoire, Michel Favre-Marinet, François Julien Saint Amand. Modeling of turbulent fluid flow over a rough wall with or with outsuction. *Journal of Fluids Engineering*, 2003, 125 (4), pp.636-642. 10.1115/1.1593705 . hal-00204630

HAL Id: hal-00204630

<https://hal.science/hal-00204630>

Submitted on 13 Feb 2020

HAL is a multi-disciplinary open access archive for the deposit and dissemination of scientific research documents, whether they are published or not. The documents may come from teaching and research institutions in France or abroad, or from public or private research centers.

L'archive ouverte pluridisciplinaire **HAL**, est destinée au dépôt et à la diffusion de documents scientifiques de niveau recherche, publiés ou non, émanant des établissements d'enseignement et de recherche français ou étrangers, des laboratoires publics ou privés.



Distributed under a Creative Commons Attribution 4.0 International License

G. Grégoire¹
M. Favre-Marinet
Laboratory of Geophysical and Industrial
Flows,
Grenoble University,
UJF-INPG-CNRS, BP 53X,
38041 Grenoble Cedex 9, France

F. Julien Saint Amand
Research Scientist,
Center Technique du Papier, BP 251,
38044 Grenoble Cedex 9, France

Modeling of Turbulent Fluid Flow Over a Rough Wall With or Without Suction

The turbulent flow close to a wall with two-dimensional roughness is computed with a two-layer zonal model. For an impermeable wall, the classical logarithmic law compares well with the numerical results if the location of the fictitious wall modeling the surface is considered at the top of the rough boundary. The model developed by Wilcox for smooth walls is modified to account for the surface roughness and gives satisfactory results, especially for the friction coefficient, for the case of boundary layer suction.

1 Introduction

Although numerical modeling of turbulent flows is continuously progressing, some questions remain open and need further investigation in many practical situations. Among them, the problem of modeling the flow over rough surface corresponds to a very common situation in industrial or geophysical applications and it has therefore received much attention from many researchers. A review of the different works on this subject can be found in Patel [1]. The simplest way of modeling high Reynolds number wall flows, and historically the oldest one, is to use a wall-function approach and to match the mean velocity profile to the logarithmic law near the wall. When a rough wall is considered, the velocity profile is well described by introducing a shift, called the roughness function and denoted ΔB , in the logarithmic law of the wall, [2,3]. Such a wall-function approach is desirable in many situations since it avoids detailed computations of the flow in the viscous sublayer and in the buffer layer and therefore saves large computation time. However, Patel [1] underlines “the uncertainty in the dependence of ΔB on the size and type of roughness and also in the effective location of the fictitious wall, from which the distance is measured.” Patel showed some inadequacy of the logarithmic law for modeling a turbulent flow over a wavy wall, which can be considered as a kind of rough surface and application of the wall-function approach is questionable for this type of surfaces.

Turbulent flows over porous walls with blowing or suction have been extensively investigated. A simple model was proposed by Stevenson [4] and in a modified version by Simpson et al. [5]. Wilcox [6] suggested modifying the von Karman’s constant and obtained results consistent with the experimental investigations of Andersen et al. [7]. However, these models did not specify the surface roughness and to our knowledge the problem of modeling a turbulent flow over a very rough wall with suction has not been considered yet.

The present study is concerned with turbulent flows over a wall with two-dimensional periodic roughness. This type of roughness is used in the paper and pulp industry and in industrial heat exchangers, for example. The purpose of this work is twofold, first to clarify the issue of the effective location of the wall for this

type of very rough impermeable surface and secondly to propose a modification of the suction or blowing laws when they are applied to such rough walls.

The flows were computed by using the FluentTM CFD software with a two-layer zonal turbulence model, which is suitable for modeling the flow in the near-wall region. The law of the wall commonly used in the wall-function approach was compared to the results of the numerical computation.

2 Numerical Approach

2.1 Flow Conditions. The present study is motivated by optimization of the flow in pressure screens, which are used in the recycling paper industry to filter the paper pulp, [8]. In these devices, the pulp is forced to pass through very fine slots (width 0.1 mm), which are machined in the screen wall in order to retain the contaminants whereas the useful fibers are entrained by the flow across the slots. In order to avoid flocculation of fibers, a tangential motion parallel to the wall is imposed to the flow (for details, see [8]). This tangential velocity component is due to the entrainment of the fluid by two-dimensional foils moving in the pulp close to the wall (typical distance: 12 mm). In a reference frame fixed to the screen wall, the flow near the surface may be considered as a steady shear layer of uniform thickness perturbed periodically by the passage of the foils. Unsteady phenomena are localized during the passage of the foils and may be disregarded during the rest of the time in a first approach. As a result, the wall region is modeled in the present study as a layer of uniform thickness submitted to steady flow conditions.

The shape of the rough wall in the present work corresponds to that of industrial pressure screens. It consists of a periodic jagged profile (Fig. 1). The geometry considered and the flow are two-dimensional. The flow rate across the slots and the flow rate of the tangential motion are adjusted independently in the computation as well as in the industrial situation. The particular case of null flow rate across the slots corresponds to impermeable wall.

2.2 Computation Domain and Boundary Conditions. The wall profile is characterized by periodic steps of height k_s , equal to 1.2 mm and of wavelength L , equal to 3.2 mm (Fig. 1). Only three waves of the pattern are considered in the computation domain. The domain height H is kept constant for all the computa-

¹Presently, Engineer, Retec, Paris, France.

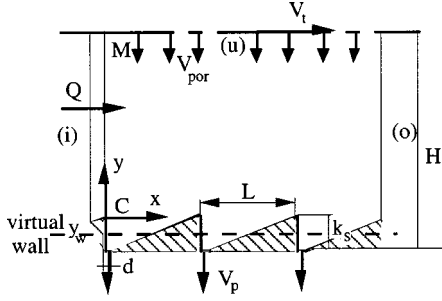


Fig. 1 Computation domain

tions, according to the assumptions discussed above. A more general case would correspond to the problem of developing boundary layers, but is not considered here.

The computed flow is assumed to be fully developed in the x -direction. It is therefore supposed to repeat periodically with the wavelength of the wall profile. Since the length of the computation domain is a multiple of the wavelength, periodic boundary conditions are assumed at the inlet and outlet sections (i) and (o) of the domain. In the case of impermeable wall, the flow rate Q per unit span across these sections is prescribed. In addition, a condition of symmetry is assumed on the upper boundary (u) of the domain, which is located at a distance H from the bottom of the troughs of the rough surface (Fig. 1).

When suction is applied through the wall, the velocity distribution in the slots is assumed to be uniform (suction velocity V_p). A uniform downward velocity V_{por} through the upper boundary is introduced in order to balance the outflow through the slots:

$$V_{por} = V_p d/L. \quad (1)$$

It is worth noting that the suction velocity V_{por} is constant along the upper boundary in keeping with the assumption that u is independent of x along the computation domain. Strictly speaking, the velocity field is periodic in x , but the influence of the jagged profile is limited to a narrow band near the surface (Section 3.1).

In the case of suction, it was no longer possible to set simultaneously a condition of symmetry and the above condition (Eq. (1)) on (u). A constant tangential velocity V_t was then assigned on (u) (details are given in Section 3.3).

2.3 Turbulence Model. The numerical computation employed the two-layer zonal model (denoted TLZM thereafter) first developed by Wolfstein [9] and later by Chen and Patel [10]. The present version is a combination of the k - ε RNG (renormalization group) model used far from the wall and a mixing length model used near the wall. The boundary between the two layers is defined by a turbulent Reynolds number, Re_{y_1} , based on the distance y_1 of a point (cell center in the numerical computation) to the nearest wall

$$Re_{y_1} = \rho k^{1/2} y_1 / \mu \quad (2)$$

where k is the turbulent kinetic energy.

For $Re_{y_1} < 200$, the one-equation model of Wolfstein is used. The turbulent viscosity is computed from

$$\begin{aligned} \mu_t &= \rho C_\mu k^{1/2} l_\mu \\ l_\mu &= c_1 y_1 (1 - \exp(-Re_{y_1}/A_\mu)). \end{aligned} \quad (3)$$

The dissipation rate ε is modeled by introducing a second length scale l_ε

$$\begin{aligned} \varepsilon &= k^{3/2} / l_\varepsilon \\ l_\varepsilon &= c_1 y_1 (1 - \exp(-Re_{y_1}/A_\varepsilon)). \end{aligned} \quad (4)$$

The constants proposed by Chen and Patel [10] are

Table 1 Influence of the grid resolution on the velocity profile over the wall crest. Differences with the results of case 4 are given in %.

y/k_s	V/V_t (Case 4)	$\Delta V/V_t$ (Case 1)	$\Delta V/V_t$ (Case 2)	$\Delta V/V_t$ (Case 3)
0.005	0.255	-6.6	-4.4	-4.2
0.106	0.382	-1.9	0.2	0.5
0.537	0.571	-2.7	0.15	0.5
4.958	0.944	-0.9	0.05	0.2

$$c_1 = \kappa C_\mu^{-3/4}, \quad A_\mu = 70, \quad A_\varepsilon = 2c_1 \quad (5)$$

with $\kappa = 0.41$, $C_\mu = 0.09$

2.4 Numerical Scheme. We employed a hybrid mesh in order to optimize accuracy while insuring a reasonable time of computation. Rectangular cells were used near the wall in order to control most efficiently the distance to the wall and to have sufficient accuracy in the viscous sublayer. At least ten cells were placed in the near wall region ($Re_{y_1} < 200$). Triangular cells were used in the external flow ($Re_{y_1} > 200$) in order to minimize the cells number while keeping a low cells skewness when the size of the cells was increased. The whole mesh consisted of about 15,000 cells.

The equations were discretized by means of a second-order accurate finite volume method. As these equations are nonlinear, a SIMPLE (semi-implicit pressure linked equations) algorithm was used. This algorithm is based on a prediction-correction method, which allows the equations to be linearized. The drawback of this iterative method is the convergence slowness. It was checked in these calculations that the number of iterations is proportional to the number of cells. The computation started with uniform values of the various physical quantities. The software FluentTM V6.0 was used on a PC HP Vectra Xu.

2.5 Numerical Accuracy. Tests were conducted for a typical case of flow with a moderate suction rate ($V_p = 3.5$ m/s, $V_t = 15$ m/s). The kinetic turbulent energy k and the rate of dissipation of the turbulent kinetic energy ε are the physical quantities, which converge with the slowest rate. The level of normalized residuals for k and ε reached 10^{-4} for both quantities after 2500 iterations, $5 \cdot 10^{-6}$ and 10^{-5} , respectively, after 10,000 iterations. Additionally, the flow rate near the wall was computed to follow the convergence of the calculations. It was defined in a cross section over a wall crest ($x=L$) by

$$q_w = \int_{y=0}^{y=0.5 \text{ mm}} u dy \quad (6)$$

The variation of q_w during 25,000 iterations showed that a minimum (-6% relative to the final value) was reached after 2500 iterations. The asymptotic value was approached with a good accuracy (+2%) after 10,000 iterations.

A first computation (case 1) was conducted with a grid of 15,700 cells, then the grid was refined in the region of high dissipation rate (downstream of the separation point at the wall crest). This case 2 used 18179 cells. Further refinement (case 3, 20,555 cells) was considered near the stagnation point, near the vortex center (Section 3.1) and in the region of high values of k . Finally, the grid of case 2 was otherwise refined (case 4, 19,118 cells) near the separation point and in the shear layer, which develops in the downstream direction behind this point. The influence of the resolution of the grid on the mean velocity profile over the wall crest was then investigated. Table 1 compares the computed values of the x -velocity with the results of case 4, which was considered as the more accurate solution, for several distances to the wall. According to Table 1, the mean velocity profile is computed with an accuracy better than 1% over most of the test section for cases 2 and 3. Errors can be estimated to 2-3% for

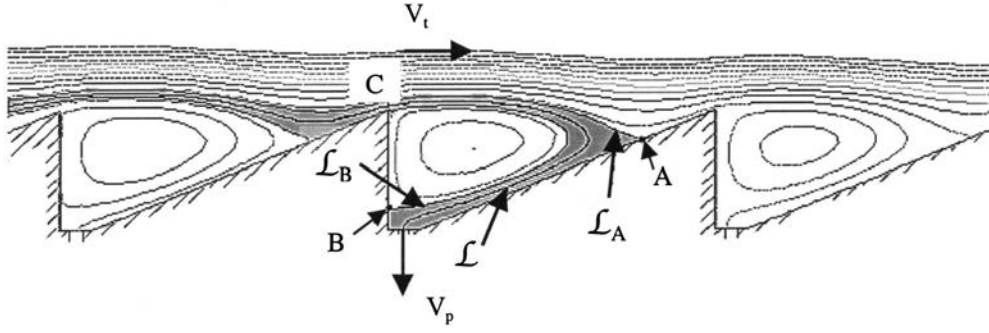


Fig. 2 Pattern of streamlines close to the screen basket. $V_p/V_t=1/3$.

case 1. The differences with the most refined case grow to 4–7% very near to the wall. The skin-friction coefficient is also slightly affected by the grid refinement (differences less than 1% between cases 2, 3 and 4, 7% between cases 1 and 4).

3 Results

3.1 Description of the Flow. A typical result showing the mean flow field is drawn in Fig. 2 for a moderate suction rate ($V_p/V_t=1/3$). The back-facing steps produce flow separation and create recirculation bubbles between two successive crests. Two particular streamlines may be considered for helping description of the flow. A streamline \mathcal{L}_A starting slightly upon a wall crest ends at a stagnation point A on the opposite side of the wall profile. On the other hand, a streamline \mathcal{L}_B starting at a wall crest C ends at a stagnation point B on the backside of the wall profile. \mathcal{L}_B is then the boundary of the recirculation bubble. \mathcal{L}_A and \mathcal{L}_B determine a streamtube corresponding to the flow through the slot. When the wall is impermeable, the flow features are essentially the same, except that only one particular streamline \mathcal{L}_A is to be considered. In this case, \mathcal{L}_A starts from C and it is the boundary of the recirculation bubble.

It is worth noting that the mean streamlines are only slightly perturbed by the wall even for small distances to the crests (Fig. 2).

3.2 Check of the Logarithmic Law for Impermeable Rough Wall. The purpose of the present section is to compare the mean velocity profile resulting from the preceding TLZM computations with the logarithmic law which is used in the wall-function approach for the case of impermeable wall ($V_p=0$). In this approach, the mean velocity profile is described in the fully rough regime, [3], by

$$u(Y)/u^* = 1/\kappa \ln(Y/k_s) + B \quad (7)$$

where u^* denotes the friction velocity equal to $\sqrt{\tau_w/\rho}$ (τ_w is the wall shear stress). $B=8.5$ for very rough walls, [3].

Y is the coordinate normal to the wall. In fluid mechanics textbooks, the origin of Y is not always clearly defined. In fact, the formulation of Eq. (7) implies that the wall is represented by a fictitious plane surface, which corresponds to the origin of Y . For very rough walls, it is crucial to clearly specify the effective location of this fictitious plane surface when using Eq. (7). The complementary issue of the present discussion concerns therefore the position of the fictitious wall which gives the best agreement of the logarithmic law with the mean velocity profile as given by the previous numerical computations. For sake of clarity, the results will be compared in a reference frame which origin is located at the top of the rough surface (point C of Fig. 1), y is the ordinate in this reference frame. If y_w denotes the location of the virtual surface introduced in the logarithmic law (Fig. 1), Y and y are related by

$$Y = y - y_w. \quad (8)$$

The mean velocity profile is then given by

$$u(y)/u^* = 1/\kappa \ln((y - y_w)/k_s) + B. \quad (9)$$

In order to compare the solutions associated to different positions of the virtual wall, u^* was adjusted for each value of y_w in Eq. (9) so as to give the prescribed mass flow rate Q through the cross section CM (Fig. 1) over a crest. The relation between Q and u^* was obtained by integrating the logarithmic law (Eq. (9)) from $y=0$ to $H - k_s$. The following relations are obtained:

$$u^* = \frac{Q}{D(H - k_s, y_w) - D(0, y_w) + B(H - k_s)} \quad (10)$$

with

$$D(y, y_w) = (y - y_w)(\ln((y - y_w)/k_s) - 1)/\kappa \quad (11)$$

$$V_t/u^* = 1/\kappa \ln[(H/k_s - 1 - y_w/k_s)] + B. \quad (12)$$

In addition, the skin-friction coefficient was obtained from the above relations by

$$C_f = 2(u^*/V_t)^2. \quad (13)$$

The equivalent coefficient was computed with TLZM by integrating the total stress exerted on the wall profile contour C in the computational domain (1: curvilinear abscissa, element of length dl).

$$C_f = \frac{1}{\rho V_t^2} \frac{1}{3L} \left(\int_C p n_x dl + \int_C \tau_x dl \right) \quad (14)$$

where p is the pressure, n_x and τ_x are, respectively, the x -components of the normal unit vector and of the computed wall shear stress. C_f includes the pressure and friction effects for this nonhorizontal surface. This definition of an equivalent friction coefficient is the same as in Taylor et al. [11]. It is here nondimensionalized with the length $3L$ of the equivalent plane virtual wall.

The above calculations were performed for $k_s=1.2$ mm, $H=12$ mm, $Q=0.15$ m³/s/m which were of industrial interest. The Reynolds number based on external velocity and half-channel height is $V_t H/\nu=2.10^5$. It should be noted that the present geometry corresponds to a very rough wall ($k_s^+ \approx 1000$).

Table 2 and Fig. 3 show the results obtained for two extreme positions of the virtual wall, at the crests ($y_w=0$) and at the

Table 2 Influence of the position of the virtual wall on the friction velocity, axis-velocity, and friction coefficient

	u^* (m/s)	$V_t(H-k)/Q$	C_f^*100
$y_w = -k$	1.131	1.15	0.99
$y_w = 0$	1.219	1.21	1.04
Numerical computations	1.21	1.20	1.04

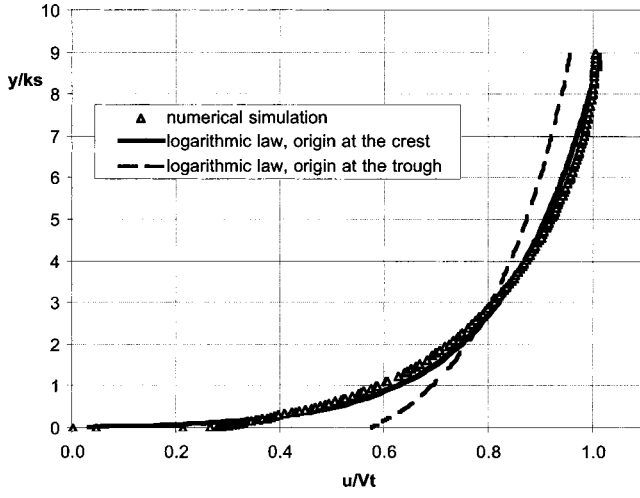


Fig. 3 Influence of the position of the virtual wall on the mean velocity profile at $x=0$

bottom of the troughs ($y_w = -k_s$) of the actual wall profile. The mean velocity profile computed over a crest by TLZM is also plotted in Fig. 3.

For this type of roughness, Fig. 3 clearly shows that the best agreement with the numerical results is obtained when the virtual wall is placed at the crests of the actual wall.

This conclusion is confirmed when computed velocity profiles are considered at three evenly distributed sections $L/3$ apart (Fig. 4). The velocity profiles almost collapse when the normalized distance to the wall, y/k_s , is higher than 0.4. Again the logarithmic law used with $y_w = 0$ (Eq. (9)) gives a good approximation of the velocity profiles. The actual mean velocity profile departs, however, significantly from the semi-logarithmic law for $y/k_s < 0.3$. Velocities are higher in this region because a mixing layer develops between the upper part of the flow and the recirculating vortex near the wall.

These results show that the details of the flow between the crests (separation, reattachment) as shown on Fig. 2, have little effect on the mean flow field at a sufficient distance ($\approx 0.4k_s$) to the wall. It is important to remark that the logarithmic plot of all the profiles uses the same mean friction velocity defined by Eq.

(13) and (14) and not the local value of the shear stress. This latter choice would have led to incoherent results since the shear stress is extremely variable on the wall and may even be equal to zero at the stagnation point A (Fig. 2).

For the case of an impermeable wall and for the present type of roughness (jagged wall profile), it may be concluded that the logarithmic law is a good approximation of the mean velocity profile over the whole rough surface. In this case, the location of the virtual wall modeling the rough surface must be taken at the top of the ridged wall.

3.3 Suction Effects. When suction is applied through the regularly spaced slots of the basket, the features of the flow are not very different from the impermeable case, as it was remarked in Section 3.1. In particular, the streamline pattern of the mean flow over the wall crests is not strongly affected by suction. Therefore, modeling suction effects over this rough wall may be tentatively undertaken by considering uniform suction through a fictitious plane porous wall. Considering the results of the impermeable case, it seems appropriate to locate this virtual wall at the crests of the wall.

The problem of suction through a smooth wall was studied by Stevenson [4] who proposed a mixing-length approach to model the flow. In this model, the mixing length is still supposed proportional to the distance to the wall whereas a source term due to suction is introduced in the momentum budget in the near-wall region. Integration in y of the x -momentum equation results in

$$\rho \kappa^2 y^2 \left| \frac{\partial u}{\partial y} \right| \left(\frac{du}{dy} \right) = \rho u^{*2} - \rho V_{\text{por}} u \quad (15)$$

where V_{por} is related to the suction velocity by Eq. (1).

Integrating Eq. (15) in y yields

$$2/V_{\text{por}}^+ ((1 + V_{\text{por}}^+ u^+)^{1/2} - 1) = 1/\kappa \ln(y^+) + C \quad (16)$$

where $V_{\text{por}}^+ = -V_{\text{por}}/u^*$.

The constant of integration C is obtained by matching Eq. (16) to the logarithmic law for smooth impermeable walls when V_{por}^+ tends to 0. This gives $C = B = 5.5$.

When a rough wall is considered and modeled by a virtual porous plane surface, the same method may be applied, but the right-hand side of Eq. (16) has to be matched with the logarithmic law corresponding to rough surfaces. In this case, we obtain

$$C = B - \Delta B = 5.5 - 1/\kappa \ln(1 + 0.3k_s^+) \quad (17)$$

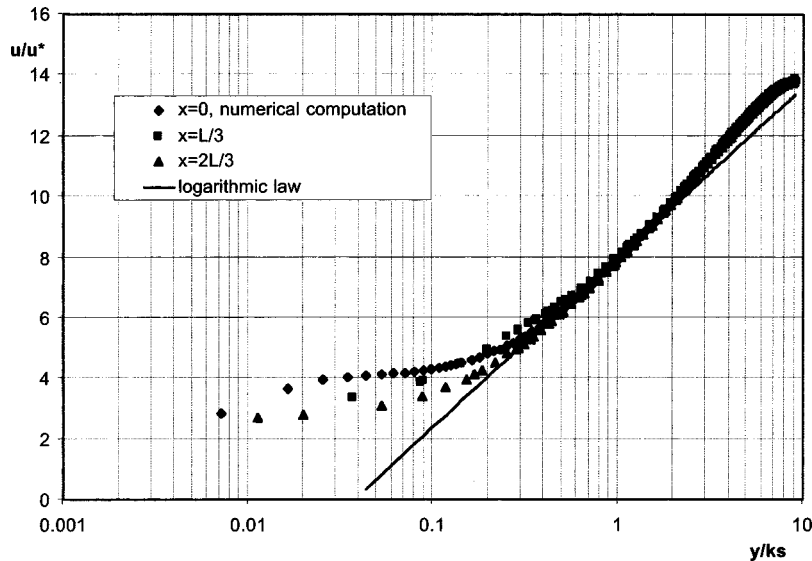


Fig. 4 Mean velocity profiles at different positions along the wall

where ΔB is the shift of the logarithmic law for a rough surface.

For the very high values of k_s^+ considered in the present study ($k_s^+ \approx 1000$), 1 is neglected in the logarithm in Eq. (17).

So finally, Stevenson's law modified for a rough surface is

$$u^+(y, k_s) = 1/\kappa \ln(y/k_s) + B - V_{\text{por}}^+ / 4(1/\kappa \ln(y/k_s) + B)^2. \quad (18)$$

We tried another approach by modifying Wilcox's formulation [6] for smooth surfaces with suction.

Starting from the experimental work of Andersen et al. [7], Wilcox obtained a good approximation of the velocity profiles by introducing the following variation of the von Karman's constant:

$$\begin{aligned} \kappa_{\text{w}} &= \kappa / (1 + \Xi V_{\text{por}}^+) \\ \text{with } \Xi &= 3.11 + 0.61 \ln(y^+) \end{aligned} \quad (19)$$

For very rough impermeable surfaces, roughness effects lead to destruction of the viscous sublayer and the distance to the wall is then correctly scaled with the roughness height k_s instead of the viscous sublayer thickness ν/u^* . Assuming the same physical process for rough surfaces with suction, we propose to modify the law of Wilcox by replacing y^+ by y/k_s in Eq. (19). The mean velocity profile is then described by

$$\begin{aligned} u^+(y, k_s) &= 1/\kappa \ln(y/k_s) + B \\ &- V_{\text{por}}^+ / \kappa (3.11 + 0.61 \ln(y/k_s)) \ln(y/k_s). \end{aligned} \quad (20)$$

The similarity between the modified Stevenson's (Eq. (18)) and Wilcox's laws (Eq. (20)) is apparent.

Using one of these two laws, it is possible to calculate the friction velocity and the flow rate across the computation domain defined in Section 2.2 if the tangential velocity V_t is given.

When the modified Stevenson's law (Eq. (18)) is used, the following expression is obtained for the friction velocity:

$$\begin{aligned} u^*/V_t &= 1/Z + Z/4V_{\text{por}}/V_t \quad (21) \\ \text{with } Z &= \lambda/\kappa + B \\ \lambda &= \ln(H/k_s - 1). \end{aligned}$$

When the modified Wilcox's law (Eq. (20)) is considered, u^* is given by

$$u^*/V_t = (1 + 1/\kappa V_{\text{por}}/V_t (3.11 + 0.61\lambda)\lambda) / Z. \quad (22)$$

The flow rate is easily deduced from the above expressions of the friction velocity u^* by integrating, respectively, the Eq. (18) and (20) over the domain height, $H - k_s$.

As in the case of impermeable wall, the flow was also computed by using the two-layer zonal model. When suction is applied through the wall, it is necessary to compensate the suction flow rate in order to keep a constant streamwise flow rate and periodic conditions on (i) and (o) (Fig. 1). This implies the introduction of a normal velocity at the boundary (u) of the flow domain. However, as mentioned before, this condition is incompatible with the previous assumption of symmetry on the upper boundary. The solution used in this simulation is then to replace the condition of symmetry on (u), by a so-called VELOCITY INLET boundary condition. This condition implies the setting of two velocity components and the turbulence quantities on (u). In this case, it is still necessary to set the streamwise flow rate Q in order to complete the boundary conditions. In the present numerical procedure, Q was computed with the modified laws of Stevenson and Wilcox (Eq. (18) and (20)). Finally, the INLET turbulent quantities introduced are the turbulence length scale and intensity usually observed in a channel flow. The computation starts with a value of 5% for the turbulence intensity on (u). This quantity is adjusted slightly during the computation by using the result obtained far from the wall.

Figure 5 compares the friction velocity u^* obtained by the above computations with the results of the TLZM numerical simu-

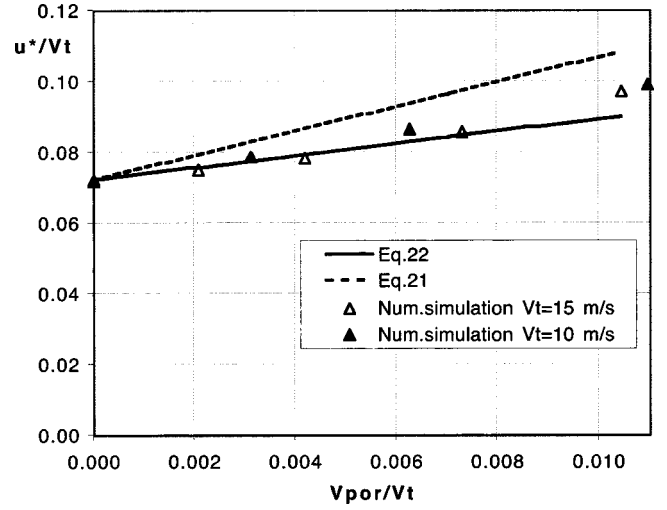


Fig. 5 Influence of suction on the friction velocity

lations for a range of suction ratios of industrial interest. u^* is given by Eqs. (13) and (14) and is normalized by the velocity V_t at the upper boundary. There is clearly an excellent agreement of TLZM results with the modified Wilcox's law (Eq. (22)) for low to moderate suction ratios. For the highest suction ratio considered in this study ($V_{\text{por}}/V_t > 0.01$), a more pronounced difference of 9% is observed between the two results. The prediction of the modified Stevenson's law overestimates the friction velocity.

It should be noted that roughness effects are stronger than suction effects for the present conditions. In fact, the nondimensionalized friction velocity was computed by using the Blasius law for a smooth wall in a channel of half-width H and center velocity V_t . Compared to this smooth wall value (≈ 0.04), the roughness effect gives a 80% increase in u^*/V_t . On the other hand, the highest suction ratio gives only a 23% increase in u^*/V_t in comparison to the rough impermeable case.

Figures 6 and 7 show mean velocity profiles over the crests computed by the different methods for two values of the suction ratio. For a moderate suction ratio ($V_{\text{por}}/V_t = 0.0073$), Fig. 6 indicates a good agreement of the TLZM results with the velocity profile given by the modified Stevenson's law (Eq. (18)). Equation (20) slightly overestimates the mean velocity. The shape of the mean velocity profile as given by TLZM is considerably modified for the highest suction ratio (Fig. 7, $V_{\text{por}}/V_t = 0.0104$). The stiffness of the velocity profile observed for $y/k_s > 3$ is accounted for by neither the modified Wilcox's law nor by the Stevenson's law. In this case, Eq. (20) (Wilcox's law) compares well with the numerical results for $y/k_s < 2$, but the corresponding velocity profile deviates significantly from the computed one in the outer part of the flow. Equation (18) does not give better agreement.

It should be remarked that the good agreement of TLZM with Eq. (18) observed in Fig. 6 deteriorates significantly when u is nondimensionalized by the friction velocity (Fig. 8). The differences in the velocity profiles reflect the discrepancy between u^* as given by the two methods.

4 Conclusions

In the present study, the flow near a ridged wall was computed by using a two-layer zonal model. The mean velocity profiles obtained by these two-dimensional computations are in very good agreement with the semi-logarithmic law for impermeable rough walls, provided the ordinate y used in this law is counted from a virtual wall located at the crests of the wall. Moreover, the friction coefficient is computed with a good approximation by using the logarithmic law throughout the flow. These results then justify the wall-function approach for this type of two-dimensional rough-

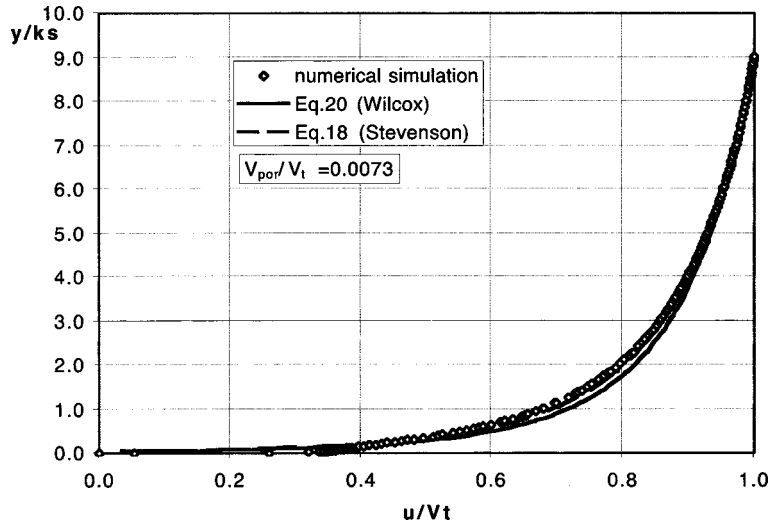


Fig. 6 Mean velocity profile at $x=0$ for a moderate suction ratio. $V_{por}/V_t=0.0073$.

ness. The shape of the wall gives rise to a sharp separation at the crests. Moreover the reattachment zone is much smaller than the separation region. This explains most likely why the best choice for the origin of the ordinate y is at the top of the rough surface ($y_w=0$). This result, which is useful for the paper and pulp industry, may also be relevant to transverse-rib roughness, which is used in tubes for enhanced heat transfer, [12]. In this case, the rib spacing will significantly affect the flow and the above conclusion should apply to small values of this parameter, which correspond to limited regions of reattachment, if any.

For three-dimensional roughness, as for Nikuradse's roughness, it is expected that the effects of separation will be weaker and consequently that the virtual origin will be located below the top of the surface ($-k_s < y_w < 0$).

The adaptation of the laws with suction from smooth to very rough walls seems also to be satisfactory if we assume that the numerical simulations are accurate. The adapted Wilcox's law gives the best results for the friction velocity and reasonable agreement for the mean velocity profiles. The proposed modification is very simple since it consists to replacing the viscous length scale by the roughness height in the modeling of the von Kar-

man's constant. Further confirmation of this model would require comparison of the present results with experiments.

The present work considered a layer of uniform thickness height, H to model the industrial problem of the flow in pressure screens. A more general case would correspond to developing turbulent boundary layers. However, longitudinal advection effects may be considered as small compared to friction effects as in Stevenson's analysis (Eq. (15)) in such flows. It is then thought that the present results would be only slightly affected by slow x -variations of H .

This method seems to be successful in the present case of two-dimensional roughness. It would be interesting to extend the conclusions of the present study in the following directions:

- further work could test the effect of the crest spacing on the position of the virtual wall.
- three-dimensional roughness could be considered, but it would require a significantly greater effort owing to the three-dimensional calculations, which would be necessary in this case.

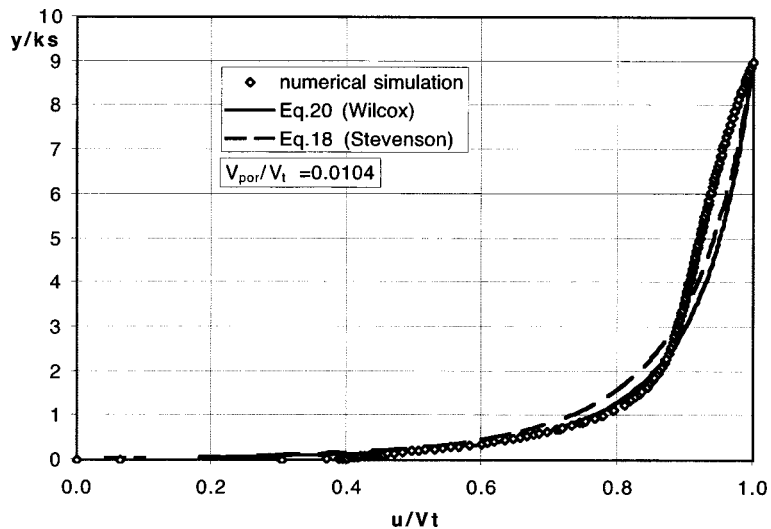


Fig. 7 Mean velocity profile at $x=0$ for a high suction ratio. $V_{por}/V_t=0.0104$.

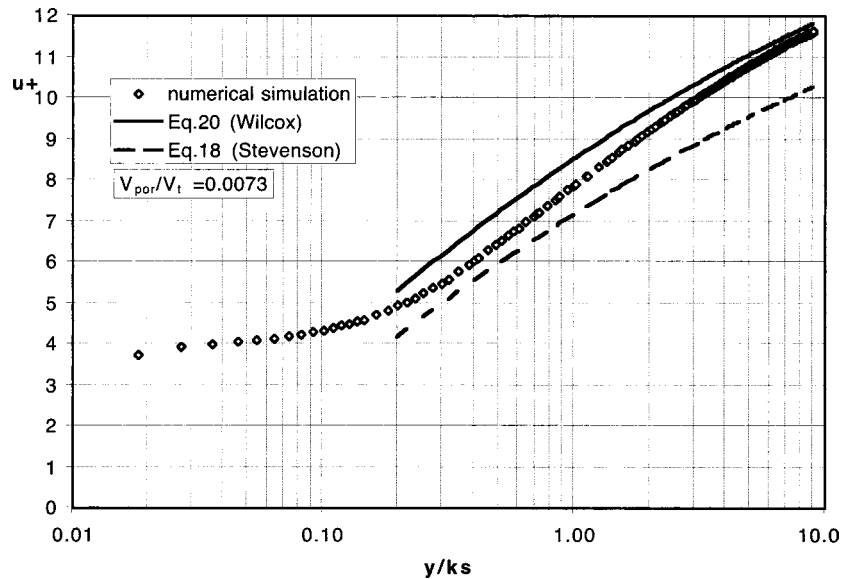


Fig. 8 Mean velocity profile at $x=0$ plotted with internal variables. $V_{por}/V_t = 0.0073$.

Acknowledgments

This research was supported by the company E.&M. LAMORT and by the French Ministry of Education, Research and Technology. Participation of Dariusz ASENDRYCH is gratefully acknowledged.

Nomenclature

- B = constant in the logarithmic law
- ΔB = roughness function
- C_f = skin-friction coefficient
- d = width of the slots
- H = height of the computation domain
- k = turbulent kinetic energy
- k_s = roughness height
- L = distance between two crests or two slots
- p = pressure
- Q = flow rate per unit length in the normal direction
- q_w = flow rate per unit length near the wall (Eq. (6))
- u = mean velocity
- u^* = friction velocity
- V_t = tangential velocity at the upper boundary of the computation domain
- V_p = suction velocity
- V_{por} = equivalent velocity for a uniformly porous wall
- x = abscissa counted from the wall crest
- y = ordinate counted from the wall crest
- y_w = ordinate of the virtual wall in the logarithmic wall
- y_1 = distance to the nearest wall
- Y = ordinate counted from the virtual wall
- ε = rate of dissipation of the turbulent kinetic energy

- κ = von Karman's constant
- ρ = fluid density
- τ_w = wall shear stress
- μ = dynamic viscosity
- ν = kinematic viscosity

References

- [1] Patel, V. C., 1998, "Perspective: Flow at High Reynolds Number and Over Rough Surfaces-Achilles Heel of CFD," *ASME J. Fluids Eng.*, **120**, pp. 434-444.
- [2] Clauser, F. H., 1956, "The Turbulent Boundary Layer," *Advances in Applied Mechanics*, **4**, Academic Press, New York.
- [3] White, F. M., 1991, *Viscous Fluid Flow*, McGraw-Hill, New York.
- [4] Stevenson, T. N., 1963, "A Law of the Wall for Turbulent Boundary Layers With Suction or Injection," Cranfield College, Aero. Report 166.
- [5] Simpson, R. L., Whitten, D. C., and Moffat, R. J., 1970, "An Experimental Study of the Turbulent Prandtl Number of Air With Injection or Suction," *Int. J. Heat Mass Transfer*, **13**, pp. 125-143.
- [6] Wilcox, D. C., 1993, "Turbulence Modeling for CFD," DCW Industries Inc., La Canada, CA.
- [7] Andersen, P. S., Kays, W. M., and Moffat, R. J., 1972, "The Turbulent Boundary Layer on a Porous Plate: An Experimental Study of the Fluid Mechanics for Adverse Free-Stream Pressure Gradients," Report No. HMT-15, Department of Mechanical Engineering, Stanford University, CA.
- [8] Marko, J. J., and LaRiviere, C. J., 1999, "The Use of Computational Fluid Dynamics (CFD) in Pressure Screen Design," *Tappi 99 Proceedings*, pp. 1477-1482.
- [9] Wolfstein, M., 1969, "The Velocity and Temperature Distribution of One-Dimensional Flow With Turbulence Augmentation and Pressure Gradient," *Int. J. Heat Mass Transfer*, **12**, pp. 301-318.
- [10] Chen, H. C., and Patel, V. C., 1988, "Near-Wall Turbulence Models for Complex Flows Including Separation," *AIAA J.*, **26**(6), pp. 641-648.
- [11] Taylor, R. P., Coleman, H. W., and Hodge, B. K., 1985, "Prediction of Turbulent Rough-Wall Skin Friction Using a Discrete Element Approach," *ASME J. Fluids Eng.*, **107**, pp. 251-257.
- [12] Webb, R. L., 1994, *Principles of Enhanced Heat Transfer*, John Wiley and Sons, New York.